Rapid NO conversion with an enhanced Sm+3–TiO2 photocatalyst

Article *in* Solid State Communications · September 2024

DOI: 10.1016/j.ssc.2024.115692

4 authors, including:

Anibal Alviz-Meza
University of Cartagena
70 PUBLICATIONS **311** CITATIONS
SEE PROFILE

Jose Colina-Márquez
University of Cartagena
58 PUBLICATIONS **1,020** CITATIONS
SEE PROFILE

Solid State Communications 394 (2024) 115692

Contents lists available at ScienceDirect

Solid State Communications

journal homepage: www.elsevier.com/locate/ssc

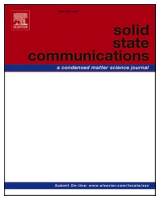

Rapid NO conversion with an enhanced Sm^{+3}-TiO_2 photocatalyst

A. Alviz-Meza [a], X. Sierra-González [a], A. Martínez-de la Cruz [b], J.A. Colina-Marquez [a,*]

[a] Department of Chemical Engineering, Universidad de Cartagena, Sede Piedra de Bolívar, Avenida del Consulado 48-152, Cartagena, A.A, 130001, Colombia
[b] Facultad de Ingeniería Mecánica y Eléctrica, FIME, Universidad Autónoma de Nuevo León, UANL, Av. Pedro de Alba s/n, Ciudad Universitaria, C.P., 66455, San Nicolas de los Garza, N.L., Mexico

ARTICLE INFO

Communicated by: Francois Peeters

Keywords:
Sol-gel
Rare earth metals
Gaseous photocatalysis
P25
Energy bandgap

ABSTRACT

Nitrogen oxides (NO_x) are known for having a significant greenhouse effect and provoking several health issues. Because of that, it is necessary to find an effective manner to remove them from polluted air. In this study, samarium-doped titania was synthesized via sol-gel using two different synthesis routes and varying the calcination temperature and the Sm^{3+} content. The main difference between the two syntheses was the pH solution. The acidic pH favored the presence of the anatase crystalline phase, the most photoactive and interesting for photocatalytic applications. Furthermore, these catalysts were evaluated in a lab-scale UV photoreactor following the NO conversion via chemiluminescence, according to the ISO standard 22197–1. The Sm content positively affected the NO removal. The highest NO conversion was 92 %, with the doped titania obtained at a calcination temperature of 500 °C and with 0.5 % wt. of samarium. This result was congruent with the reported literature's energy bandgap estimated (2.98 eV).

1. Introduction

Nitrogen oxides, or NO_x, are some of the most prevalent pollutants present in the air. NO_x gases in vehicles' emissions can generate ozone/photochemical fog, solid particles, acid rain, and carcinogenic products. All these issues affect the sustainability of life and the environment [1]. People exposed to high NO_x levels in urban zones with many vehicles can exhibit nose, eyes, lung, and throat irritations [2]. Other symptoms are cough, nausea, and tiredness, which may become lung affections [3]. In addition, industries contribute to air pollution with NO_x gases by employing low air excess combustion processes and recirculating their associated gases.

These environmental and health affections have motivated several studies that propose mechanisms to remove NO_x from air-charged streams. For example, some industries have adopted post-combustion techniques, such as non-catalytic selective reduction and selective catalytic reduction (SCR), as treatments to reduce NO_x emissions [4,5]. For instance, previous studies reported Pd/Co catalyzers and a natural iron zeolite for NO removal, reaching reductions of up to 86 % and 42 %, respectively [4,6]. These high NO conversions are very promising; however, these conversions drop after long times of reaction. The reaction mechanisms with these catalysts are not favorable to guarantee the final products' stability, and the final NO conversions obtained become unsatisfactory.

Semiconductor-based photocatalysis emerges as one of the most attractive alternatives for removing NO_x from air streams. Several studies have reported satisfactory performances of different semiconductors in the photocatalytic oxidation of NO [7–10]. One of the most essential features is UV radiation as a photon source to promote redox reaction with the presence of an oxidant. For this reason, it is very relevant that the semiconductor can absorb the most significant number of UV photons possible to ensure an excellent photocatalytic degradation performance. Conversely, several reports show that heterogeneous photocatalysis can achieve 100 % efficiency for NO_x removal from flue gases [10–12].

Gas-phase photocatalysis includes photo-decomposition, photooxidation, and photo-selective catalytic reduction. Photocatalysis is the most recommendable of these three processes for removing NO_x from large air volumes. In photocatalytic oxidation, reactive oxidant species (ROS) oxidize NO to HNO_3 and NO_2, where alkaline or alkaline earth metal ions neutralize them to nitrates [13]. Based on this premise, searching for a proper semiconductor is one of the primary targets of the reported studies on NO_x photocatalytic elimination.

Todorova et al. [14] tested films of ZnO, TiO_2, and a composite of TiO_2/ZnO to reduce NO_x. As a remarkable result, the samples with pure anatase crystalline showed the best performances, and the presence of

* Corresponding author.
E-mail address: jcolinam@unicartagena.edu.co (J.A. Colina-Marquez).

https://doi.org/10.1016/j.ssc.2024.115692
Received 13 June 2024; Received in revised form 31 August 2024; Accepted 7 September 2024
Available online 8 September 2024

the ZnO in the composite film was detrimental to the photocatalytic activity. Nonetheless, they used a TiO_2/ZnO film modified with Pluronic F27, and the photocatalytic performance improved significantly, even overcoming the one obtained with the pure TiO_2 film. Previously, the same researchers had tested a titania catalyst modified with clays. In this case, the modified titania showed worse results than the unmodified catalyst [15].

Modifying the titania catalyst via coating with other semiconductors or doping with metals or non-metals are the preferred techniques for improving photocatalytic performance for aqueous and gas-phase reactions. In this way, the search for better photocatalytic performances has focused on synthesizing visible-light active (VLA) materials. Martínez-Oviedo et al. [16] developed a Sn-doped blue TiO_2 that exhibited excellent effectiveness for NO_x abatement. This modified titania achieved a NO removal of 60 % after 60 min of solar irradiation. As mentioned previously, UV radiation is a critical factor for the performance of photochemical reactions, so the possibility of using solar UV photons of the visible spectrum is a strategic advantage for outdoor applications. These VLA catalysts are obtained mainly by metal or non-metal titania doping; nonetheless, most of these works have focused on contaminants' removal in the aqueous phase. From these works, the use of rare-earth metals remarks as an alternative to broaden the visible spectrum of radiation and its activity [17–22]. Arévalo-Pérez et al. and De la Cruz et al. reported satisfactory photocatalytic degradations of pesticides in water by using Sm^{+3}-doped titania [23,24]. Samarium reduced the TiO_2 band gap and successfully extended its radiation absorption into the visible light spectrum [24]. This feature favors the degradation of various pollutants with comparable or better yields than commercial catalysts. The use of rare earth-doped titania for photocatalytic removal of pollutants in the gas phase has also shown promising results [25,26]. Tang et al. [27] obtained remarkable acetone and methanol eliminations in the gas phase with Sm-doped titania, synthesized via sol-gel with a template of Pluronic P123. In this study, the synthesized material outperformed P25 in removing these pollutants due to the presence of samarium. Sm-doping has a beneficial effect on TiO_2 photoactivity due to the augmented efficiency of charge separation. Di Paola et al. [28] obtained interesting results with pollutants in gas and liquid phases with Sm-doped brookite. Conversely, Chang et al. [29] studied the charge separation in Sm-doped titania using surface photovoltage spectroscopy (SPV), which contributed to understanding photoactivity enhancement. Kutuzova et al. showed that Sm content significantly affects the modified titania photoactivity, with an optimal range of 0.5–1.0 % w/w [30].

In this work, two sol-gel synthesis routes were used to obtain Sm-doped titania. The solution's pH strongly affected the development of TiO_2 crystalline phases, and the Sm content influenced the photocatalytic NO_x elimination. As a noteworthy result, the NO conversion obtained with the modified titania was higher than with the commercial catalyst P25.

2. Materials and methods

2.1. Synthesis of Sm-doped TiO_2 catalyst

Two sol-gel synthesis routes were used to produce the Sm-doped titania. Route 1 employed a procedure with pH control, and route 2 used one without controlling the pH of the synthesis reaction. Route 1 showed promising results with syntheses of TiO_2 modified with rare-earth elements, and the samarium exhibited the best photocatalytic activity among them [31]. The two synthesis routes used samarium nitrate (analytical reagent grade, MERCK®).

Route 1: Arévalo-Pérez et al. reported the procedure for this synthesis [23], as seen in Fig. 1. The first solution for the synthesis (solution A) was prepared by adding 3.7 mL of titanium isopropoxide dropwise to 7.5 mL of propanol within a glass container. Solution A needed to be stirred and heated to 70 °C. The second solution (solution B) was prepared by adding the samarium nitrate with 10 mL of deionized water and 2.6 mL of propanol. The amount of Sm nitrate depended on the concentration desired for the doped catalyst (0.1, 0.3, and 0.5 % wt.) and the final amount of titania expected after the synthesis. Solution B was dropwise added to solution A with uniform stirring and heating. The solution preparation continued by adding ammonium hydroxide to the resultant solution until it reached a pH of 7. This solution was kept under constant heating and stirring for 24 h until the formation of a gel. After that, the gel was dried at 120 °C for 12 h (in an oven) and pulverized later. Finally, the samples were calcined in an electric furnace for three hours at 400 °C, 450 °C, and 500 °C.

Route 2: Luévano-Hipólito and Martínez reported the procedure used in this synthesis method, as seen in Fig. 2 [32]. Solution A was prepared with 3.7 mL of titanium isopropoxide and 10 mL of absolute ethanol (DEQ 99 %), which was stirred for 30 min. Then, the samarium nitrate solutions were added to 10 mL of distilled water and 10 mL of glacial acetic acid to obtain the above Sm concentrations. The obtained gel was stirred for one hour to initiate the hydrolysis and condensation reactions, aging it for one day at room temperature (25-27 °C). The gel obtained was dried at 100 °C for 24 h to remove the solvent until a beige powder was obtained. Lastly, the sample was calcined at 400 °C, 450 °C, and 500 °C, following the experimental procedure previously cited.

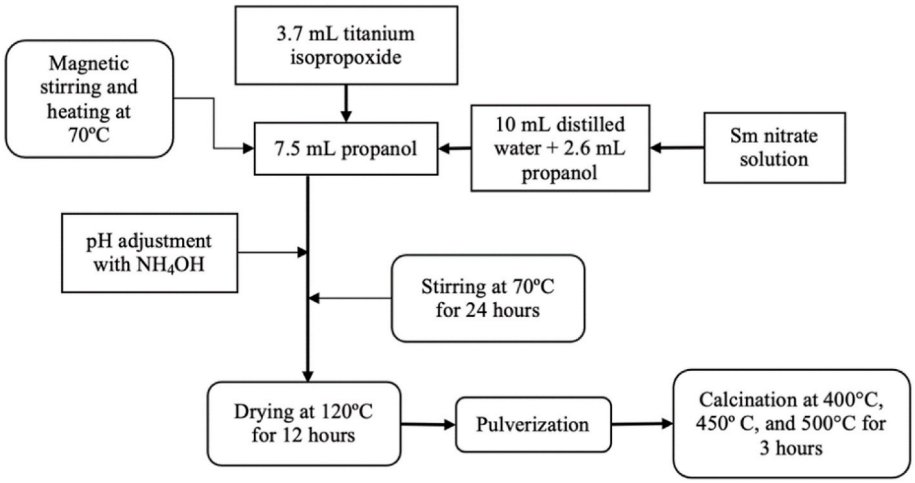

Fig. 1. Procedure for route 1 of Sm-doped titania synthesis.

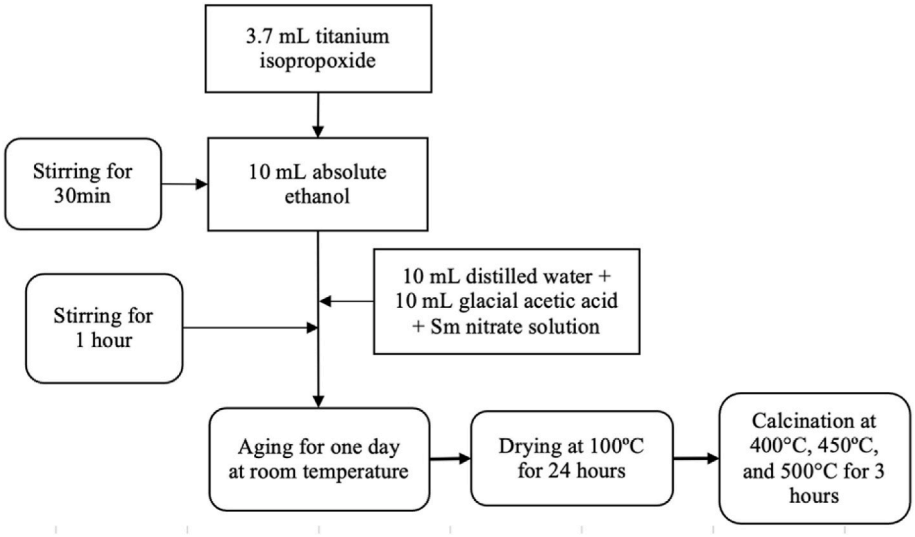

Fig. 2. Procedure for route 2 for Sm-doped titania synthesis.

2.2. Characterization of synthesized Sm-doped titania

X-ray powder diffraction (XRD) and Diffuse reflectance spectroscopy (DRS) were performed to define the most relevant characteristics of the synthesized materials. XRD determines the crystallinity of the materials by comparing the intensities of their primary reflections with those of reference samples. These analyses were conducted in a Bruker D8 Advance model diffractometer equipped with Cu radiation (Kα = 1.5405 Å), operated at 40 kV and 30 mA. The crystal structures were identified with the JCPDS library.

On the other hand, DRS estimates the spectrum of UV radiation absorption by a solid sample. This analysis was conducted in an Agilent Technologies UV–Vis–NIR spectrophotometer model Cary 5000 series. This equipment has an accessory with a diffuse reflectance integrating sphere, using polytetrafluoroethylene as a reference. The samples needed to be pulverized and self-supported in the polymeric material for the analysis. The UV absorption data measured by the DRS equipment were processed through the Kubelka-Munk function. The UV spectrophotometer recorded UV absorption data within a wavelength range from 200 to 800 nm, with a step size of 1 nm. This technique allowed us to measure the energy bandgap energy of the catalysts, applying the baseline method used for doped semiconductors [32].

2.3. Photocatalytic experiments

The photoreactor consisted of a top window to allow the UV radiation to pass to the solid catalyst sample, with a stainless-steel frame and 0.8 L of total reaction volume. In a typical experiment, 100 mg of the sample was dispersed with ethanol on a 0.08 m^2 glass support. This recipient's dimensions were 5 mm wide and 10 mm long. Inside the photoreactor, two 20-W black lamps (TecnoLite) irradiated the samples with a 365–400 nm UV spectrum. A CR 10 digital radiometer was used

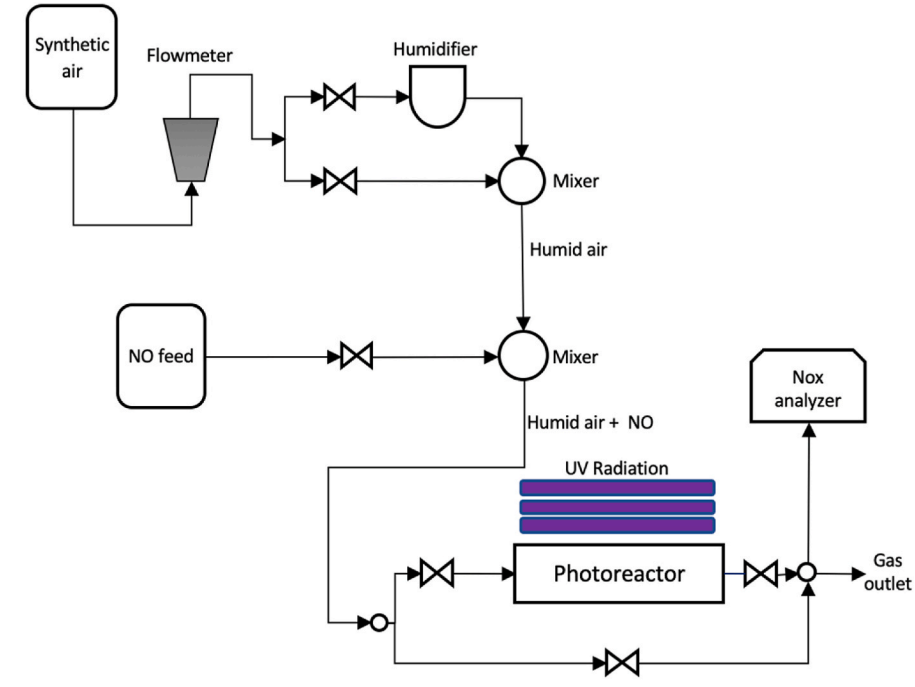

Fig. 3. Experimental setup for lab-scale photooxidation of NO.

to measure the UV radiation received by the catalyst samples.

The synthetic air consisted of 20.5%v/v of O_2 and 79.5%v/v of N_2. A relative humidity of 70 % was maintained with a humidifier. These two streams were mixed to obtain humid air. A 3-ppm of NO feed, stabilized in N_2, was used as inlet gas to the reactive system. NO concentration was adjusted to 1 ppm by adding the synthetic air stream, and the gas flow rate was adjusted to 1 L/min. Subsequently, the gas flow was inserted into the photoreactor to evaluate the activity of the catalyst, Fig. 3. The UV lamps irradiated the synthesized samples for 30 min. The UV radiation intensity was 8.2 W/m^2, measured at the center of the photocatalytic reactor. Finally, a chemiluminescence system (EcoPhysics 88p analyzer) was employed to record NO_x outlet concentrations according to the procedure of the international standard ISO 22197–1 [33].

The design of experiments consisted of a 2^2-factorial system, including one central point (see Table 1) to evaluate the effect of calcination temperature and Sm^{+3} concentration on the NO photocatalytic removal. The calcination temperatures used were 400, 450, and 500 °C, while the Sm^{+3} concentrations were 0.1, 0.3, and 0.5 % wt. The software Statgraphics XVI® (Trial version, Statgraphics) was used to obtain the variance analysis (ANOVA) and the Pareto chart. The results obtained were compared with the literature based on the similarities of the methods.

A kinetic analysis was also carried out to determine the constants of a Langmuir-Hinshelwood rate law. The parameters could be estimated from a linear regression analysis of the experimental data corresponding to the photocatalytic tests with the R2 samples. This analysis aimed to compare the kinetic constants of these modified titania samples with those reported by Luévano-Hipólito and Martínez De La Cruz [32]. In the cited research, bare titania samples were tested to remove NO from a synthetic air stream under the same experimental conditions of this study.

3. Results and discussion

3.1. Crystalline phases of the Sm-doped titania

The main target of titania synthesis was to obtain the anatase phase in a majoritarian proportion. However, the samples synthesized by controlling pH exhibited the presence of the undesired brookite phase (see Figs. S1–S5 in the Supporting information section). The brookite presence depended strongly on the pH of the sol-gel synthesis, and the content of this phase increased as the solution pH solution was increased [34]. This behavior is explained by the interaction of the solution pH with water content and temperature. Titania crystallinity is affected by these synthesis parameters, and more crystalline structures are present at lower pH values. Whereas crystalline titania favors the anatase phase, amorphous TiO_2 exhibits significant brookite contents [35]. Route 1 (pH-controlled) used ammonium hydroxide to neutralize the synthesis solution, whereas route 2 allowed pH derivation. For route 1, the additional water used to adjust the pH favored the presence of amorphous structures because of the lattice loosening and reduction of gelation time. The brookite phase appears as an initial rutile phase transition under such synthesis conditions [35]. Conversely, the pH solution of route 2 was around 3–5 because of the acetic acid addition, and anatase was the predominant crystalline phase of the catalyst, as seen in Fig. 4. Additionally, replicating the experimental procedure for route 1 was challenging since the pH changed after being adjusted under neutral values [36,37].

Concerning calcination temperatures and Sm content, they did not affect the content of the anatase crystalline phase in any of the samples (route 2). Regarding calcination temperature, the rutile phase did not appear because these temperatures were under 500 °C [38]. The Sm content did not affect the crystallinity degree because of the low concentration of the dopant. The lattice imperfections due to the doping did not represent significant changes in the catalyst structure. Since only route 2 obtained samples without the brookite phase (tagged as "R2″), DRS analyses and photocatalytic tests were performed with the titania samples synthesized via route 2.

Table 1
Experimental design.

Tests	Factors	
	A (°C)	B (%wt.)
1	400	0.1
2	400	0.5
3	450	0.3
4	500	0.1
5	500	0.5

3.2. Energy bandgap of Sm-doped titania samples

Table 2 shows the energy band gap of the samples synthesized via route 2 and calculated by the baseline method from the UV–Vis DRS analyses (see Figs. S6–S10 in the Supporting Information). The results showed that Sm-doped titania energy bandgap decreases as Sm^{+3} concentration increases. The introduction of Sm^{+3} ions narrowed the gap between the valence and conduction bands of the TiO_2 catalyst. The 4f electrons of the rare earth elements and their transitions with the conduction or valence bands of TiO_2 are responsible for the bandgap shifts [39–41]. The TiO_2 energy bandgap decreased when the Sm concentration increased because there was a more intense charge transfer between the TiO_2 and the samarium ions incorporated within the semiconductor lattice [41]. On top of that, the reason for the observed behavior is the promotion of impurities' energy levels in the band structure of the host due to the inclusion of rare earth ions [40].

The contraction of the bandgap in the TiO_2 catalyst facilitates the electron transfer from the valence band to the conduction band [41]. Hence, the sample with the lowest energy bandgap (0.5Sm-500°C-R2) should perform the best during the photocatalytic degradation of NO_x gases. In addition, the energy bandgap of this sample is lesser than the undoped titania's (3.2 eV), so the modified titania can absorb radiation in the UV–visible spectrum [24]. On the other hand, the Sm content positively affects the energy bandgap. Increasing the dopant concentration decreased the energy bandgap because of the larger quantity of

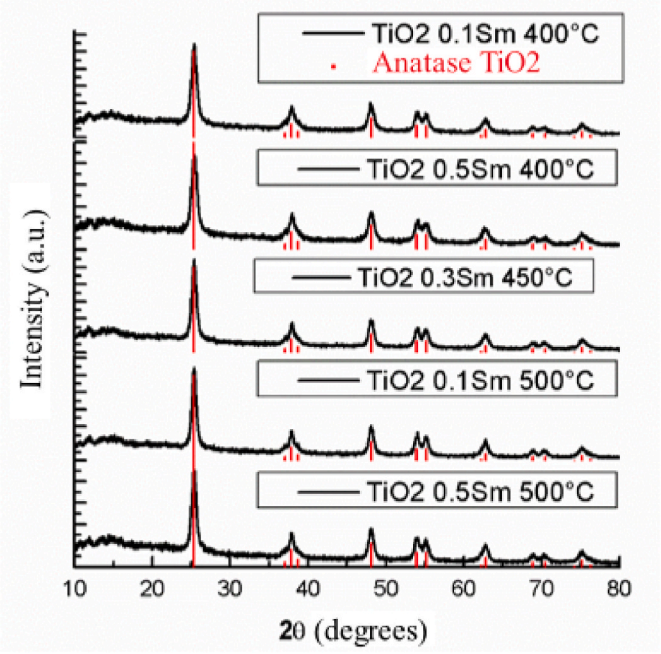

Fig. 4. XRD pattern of Sm-doped titania synthesized via route 2.

Table 2
Bandgap energy values for Sm-doped titania synthesized via route 2.

Sample (%wt. Sm)	Energy bandgap (eV)
0.1Sm-400°C-R2	3.15
0.5Sm-400°C-R2	3.06
0.3Sm-450°C-R2	3.08
0.1Sm-500°C-R2	3.09
0.5Sm-500°C-R2	2.98

modified active sites on the catalyst surface [22,41,42].

3.3. Photocatalytic oxidation of NO_x

The 0.5%Sm-500°C-R2 catalyst delivered the highest photooxidation of NO_x, achieving a 92 % NO conversion (see Fig. 5). The obtained result is congruent with the energy bandgap of this sample. Higher pollutant removals were obtained when samarium content increased within the TiO_2 catalyst, which is congruent with the previous results of the bandgap energies [26]. However, concentrations of rare-earth dopants above 0.5 % w/w may reduce the TiO_2 catalyst performance. This phenomenon is related to substrate adsorption on the catalyst surface since the molecules of the pollutant compete for the active sites occupied by the dopant [42–44].

The calcination temperature also played a differential role in photocatalytic reaction with rare-earth doped TiO_2 catalysts, where 500 °C and 550 °C were the reported conditions with better results [24,26,27,44–46]. Typically, photocatalytic performance decreases with increasing calcination temperature [42,47,48]. As mentioned previously, the presence of determined crystalline phases depended on the calcination temperature, and the pure or quasi-pure rutile phase appears with calcination temperatures over 500 °C. In addition, certain anatase-rutile phase mixtures, such as the commercial catalyst P25, promote photocatalytic activity [48]. Nevertheless, Wang et al. [49] suggested that a pure anatase phase can yield higher photocatalytic conversions of NO_x. Therefore, our results are congruent with the reported scientific literature considering the effect of calcination temperature on photocatalytic performance [27].

Considering the route used by Luévano-Hipólito et al. [32], the results obtained in this study are comparable to the ones reported in the cited work. Their best results reached 91.3 % of NO conversion in the pseudo-stationary region (after 40 min) with the same amount of TiO_2 used (100 mg), whereas, in this work, the highest NO conversion was 92 % after 5 min (as seen in Fig. 5). The increase of Sm content also favored the NO conversion, as expected from the energy bandgap estimated previously.

The set of reactions (Eqs. (1)-7)) proposed by Luévano-Hipólito and Martínez De La Cruz [32] explained the degradation route of NO conversion to NO_3^- ions. Conversely, Eqs. 8 and 9 show the Sm^{+3} interaction in the photocatalytic process, avoiding the recombination of electron-hole pairs, as proposed by Peng et al. [26].

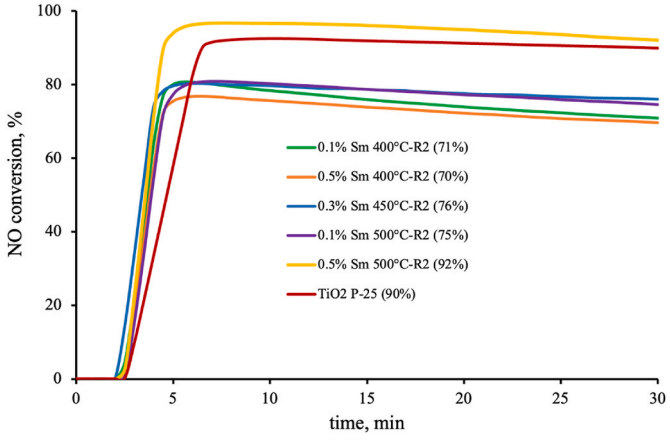

Fig. 5. NO conversion with Sm^{+3}-TiO_2 catalysts.

$$TiO_2(s) + h\nu \rightarrow TiO_2\left(e^-_{CB}\right) + TiO_2\left(h^+_{VB}\right) \quad (1)$$

$$TiO_2\left(h^+_{VB}\right) + H_2O_{ads} \rightarrow OH^*_{ads} + H^+ + TiO_2(s) \quad (2)$$

$$TiO_2\left(e^-_{CB}\right) + O_{2ads} \rightarrow O^{*-}_{2ads} \quad (3)$$

$$NO(g) + OH^*_{ads} \rightarrow HNO_2(l) \quad (4)$$

$$HNO_2(l) + OH^*_{ads} \rightarrow NO_2(g) + H_2O(l) \quad (5)$$

$$NO_2(g) + OH^*_{ads} \rightarrow NO_3^- + H^+ \quad (6)$$

$$NO(g) + O^{*-}_{2ads} \rightarrow NO_3^- \quad (7)$$

$$Sm^{+3} + e^- \rightarrow Sm^{+2} \quad (8)$$

$$Sm^{+2} + O_2 \rightarrow Sm^{+3} + O_2^- \quad (9)$$

Equations (1)–(3) describe the mechanism for electron-holes pair photogeneration, hydroxyl free radicals, and superoxide radicals' formation. The hydroxyl and superoxide radicals oxidize NO to HNO_2 and NO_3^-, respectively. Nonetheless, the HNO_2 is oxidized to NO_3^- as seen in Eqs. (5)–(7). Luévano-Hipólito and Martínez De La Cruz [32] reported that the conversion to NO_3^- was 85.0 % (with an overall conversion of 91.3 %) under the same experimental conditions of this study. According to this research, the water content in the synthetic air favored the NO conversion to NO_3^- significantly.

Eqs. (4)–(6) describe the NO_2 formation that is responsible for the presence of the pseudo-stationary state in NO removal. Since the NOx analysis by chemiluminescence detects and quantifies NO and NO_2 as a NOx gas mixture when the NO_2 is formed, the NO conversion measured reaches a plateau and can exhibit a decrease in some cases.

Although the Sm presence does not affect the NO conversion mechanism, Eqs. 8 and 9 show that the Sm dopant competes with the oxidant for the electrons generated by photo-excitation. Although this phenomenon can reduce the amount of OH· radicals, the generated superoxide anions emerge as alternative oxidant species.

Moreover, the enhancement of the NO conversion with the Sm-doped was more evident when compared with the NO photooxidation with the P-25 commercial catalyst. Luévano-Hipólito and Martínez De La Cruz reported [50] a NO removal of 90 % with P-25 titania under the same experimental conditions used in this study, except for the amount of catalyst in the photoreactor. The cited study used 50 mg of P25 commercial study against 100 mg of Sm-doped titania. The NO conversion reached the pseudo-stationary state more rapidly with the modified titania than with P25 commercial TiO_2 because of this difference in catalyst amount. Conversely, this result confirms that the sole anatase phase is more effective than the rutile-anatase mixture for NO_x photooxidation, as suggested by Wang et al. [49]. The anatase is more active than the rutile phase because of its larger surface area. This feature benefits the NO removal but not the NO_2 selectivity; although this latter can be a drawback, the overall effect is positive. In this case, the samarium could play a relevant role in the selective oxidation of the photoreaction by-products due to its affinity with the electron of the photogenerated pair.

3.4. Kinetic analysis

The Langmuir-Hinshelwood (L-H) parameters were estimated from the rate law (Eq. (9)) and the mass balance for a piston-flow reactor (Eq. (10)):

$$-r_{NO} = \frac{kK_D C_{NO}}{1 + K_D C_{NO}} \tag{9a}$$

$$FA_0 dX_{NO} = -r_{NO} dV \tag{10}$$

where $-r_{NO}$ is the reaction rate (mg/m^3·s), k is the kinetic constant (mg/m^3·s), K_D is the adsorption constant (m^3/mg), C_{NO} is the NO concentration (mg/m^3), F is the surface mass surface (mg/m^2·s), A_0 is the reactor cross-sectional area (m^2), X_{NO} is the NO conversion, and V is the reactor volume (m^3). Eq. (11) represents the NO conversion expressed in terms of inlet and outlet NO concentrations:

$$X_{NO} = \frac{C_{NO,in} - C_{NO,out}}{C_{NO,in}} \tag{11}$$

The $C_{NO,out}$ corresponds to the NO concentration that varies with reaction time, and the inlet concentration was considered constant (approximately 1000 mg/m^3). So, the $C_{NO,out}$ will be represented as C_{NO} from this point. Substituting Eqs. (9) and (11) in Eq. (10), the following expression is obtained:

$$\frac{C_{NO,in} V}{FA_0} = -\frac{1 + K_D C_{NO}}{kK_D C_{NO}} dC_{NO} \tag{12}$$

The inlet flowrate (Q) can be obtained from the following equation:

$$Q = \frac{FA_0}{C_{No,in}} \tag{13}$$

Eq. (12) can be integrated by setting the limits of C_{NO} as outlet and inlet concentrations of the photocatalytic reactors:

$$\frac{V}{Q} = \frac{1}{kK_D} \ln \frac{C_{NO,in}}{C_{NO,out}} + \frac{C_{NO,in} - C_{NO,out}}{k} \tag{14}$$

Eq. (14) can be rearranged to fit a linear expression that is used to estimate the L-H parameters:

$$\frac{V}{Q} \cdot \frac{1}{C_{NO,in} - C_{NO,out}} = \frac{1}{kK_D} \ln \frac{C_{NO,in}}{C_{NO,out}} \cdot \frac{1}{C_{NO,in} - C_{NO,out}} + \frac{1}{k} \tag{15}$$

Eq. (15) follows the general expression $y = mx + b$, where the slope m corresponds to $1/kK_D$ and the y-intercept b is $1/k$. Thus, the experimental data of the photocatalytic experiments were plotted to find the L-H parameters from a linear regression analysis (Fig. 6).

Table 3 shows the kinetic and adsorption constants estimated from fitting the experimental data of photocatalytic NO removal tests. The Sm content positively affected the reaction rate since 0.3 % and 0.5 % exhibited the highest kinetic constants (k). The calcination temperature also has a positive effect.

The adsorption constants (K_D) results were similar; only the 0.5%Sm 500°C-R2 sample presented a higher result. As $K_D C_{NO}$ >1.0, the adsorption stage in the photocatalytic reaction is not neglectable. Strong adsorption contributes to a faster NO removal because it favors the redox reactions on the catalyst surface.

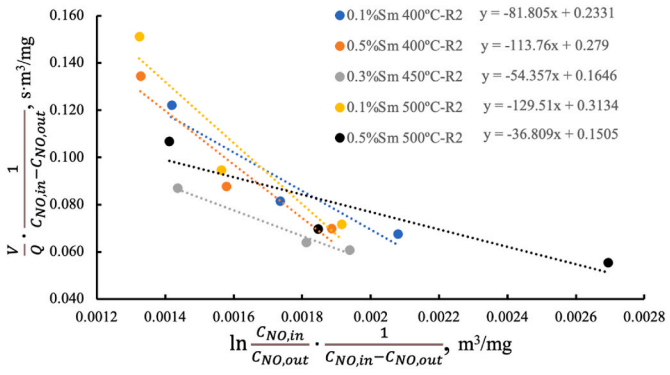

Fig. 6. Linear regression analysis for kinetic analysis of NO photocatalytic removal.

Table 3
Kinetic and adsorption constants for NO removal.

Sample	k (mg/m^3·s)	K_D(m^3/mg)
0.1 % Sm 400°C-R2	4.29	0.0028
0.5 % Sm 400°C-R2	3.58	0.0025
0.3 % Sm 450°C-R2	6.08	0.0030
0.1 % Sm 500°C-R2	3.19	0.0024
0.5 % Sm 500°C-R2	6.64	0.0041

Comparing these results with those of the reference study of Luévano-Hipólito and Martínez-De La Cruz [32], the best kinetic constant of this work is two magnitude orders higher than the estimated in the cited research (0.02 mg/m^3·s). Nonetheless, the adsorption constant of the referenced work is three magnitude orders higher than the estimated in this study. The Sm presence enhanced the TiO_2 photoactivity, increasing the hydroxyl free radical's generation and the NO removal reaction rate.

These results are congruent with the bandgap energies reported previously (Table 2). The reduction of the bandgap energy favored the UV photon absorption and decreased the electron-hole pair recombination rate [16]. This behavior represented an enhanced photocatalytic performance of the modified TiO_2.

3.5. Effects of Sm concentrations and calcination temperatures on NO_x photooxidation

An analysis of variance (ANOVA) was carried out to assess the influence of the Sm concentrations and calcination temperatures on NO photooxidation, as shown in Table 4.

These results showed that only the temperature and the interaction of both factors significantly influence the conversion degree of NO, considering a significance level of 0.05. Meanwhile, the null hypothesis (H_0) for samarium concentration cannot be rejected, implying that this factor did not statistically affect the photocatalytic NO conversion.

The Pareto chart (Fig. 7) also shows the signs of the effects and the interaction. This figure indicates that calcination temperature influences the NO removal positively, meaning that if the calcination temperature increases, the NO conversion will do the same. On the other hand, the interaction of calcination temperature and Sm concentration leads to a synergistic effect. This interaction means that by increasing both factors simultaneously, NO conversion will increase significantly more than if the factors increased separately.

The results of both statistical tools are consistent with the experimental data in Fig. 5. Although the effect of Sm content is statistically insignificant, the synergistic interaction suggests that this variable is relevant to the performance of the synthesized catalyst. This analysis shows that the synthesis appreciably affected the photocatalytic performance since relevant parameters such as the energy bandgap and the crystalline phase depended strongly on the calcination temperatures and Sm concentrations.

4. Conclusions

The synthesis route without pH controlling (R2) was the most suitable for the obtained crystalline phases of titanium dioxide since neutral

Table 4
ANOVA of NO_x photooxidation.

Source	Sum of Squares	Gl	Mean SS	F-Ratio	p-Value
A: %Sm	66.42	1	66.42	157.96	0.0505
B: Temperature	170.30	1	170.30	405.00	0.0316
AB: Interaction	87.42	1	87.42	207.90	0.0441
Total error	0.43	1	0.43		
Total (corr.)	324.57	4			

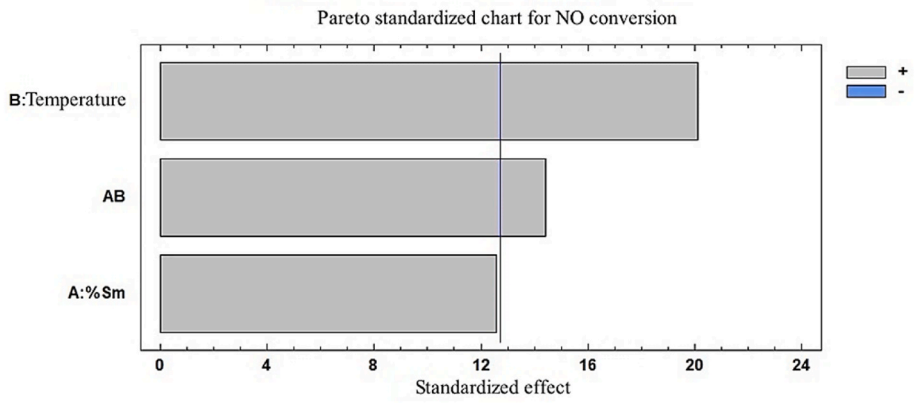

Fig. 7. Pareto chart for NO conversion.

pH favored the presence of the undesired brookite phase. The titania modification with samarium yields satisfactory results regarding the energy bandgap of the semiconductor and, consequently, the NO conversion. The synthesis conditions that favored the photocatalytic performance were 0.5 % wt. of samarium and 500 °C of calcination temperature. This titania phase and its crystallinity degree allowed it to achieve high and faster NO conversions, outperforming the commercial catalyst P25. The presence of Sm improved the photocatalytic performance of TiO_2 when compared with bare TiO2 obtained under the same experimental conditions. The reaction rate increased significantly thanks to the enhanced photoactivity of the modified titania.

CRediT authorship contribution statement

A. Alviz-Meza: Writing – review & editing. **X. Sierra-González:** Writing – review & editing, Investigation, Formal analysis, Data curation. **A. Martínez-de la Cruz:** Writing – review & editing, Resources, Formal analysis, Conceptualization. **J.A. Colina-Marquez:** Writing – review & editing, Supervision, Project administration, Conceptualization.

Declaration of competing interest

The authors declare that they have no known competing financial interests or personal relationships that could have appeared to influence the work reported in this paper.

Data availability

No data was used for the research described in the article.

Acknowledgments

The authors thank Minciencias-Colombia for financing the post-doctoral researcher A. Alviz-Meza in call 639 of 2021. Prof. Martínez-De la Cruz thanks Universidad Autónoma de Nuevo León (UANL, México) for facilitating the laboratories and materials required for synthesizing catalysts, characterization, and photocatalytic evaluation. Also, Prof. Colina-Márquez thanks the University of Cartagena (Colombia) for financially supporting the research project 088–2019.

Appendix A. Supplementary data

Supplementary data to this article can be found online at https://doi.org/10.1016/j.ssc.2024.115692.

References

[1] L. Zeng, J. Yang, H. Guo, X. Lyu, Impact of NOx reduction on long-term surface ozone pollution in roadside and suburban Hong Kong: field measurements and model simulations, Chemosphere 302 (2022) 134816.
[2] P. Amoatey, H. Omidvarborna, M.S. Baawain, A. Al-Mamun, Emissions and exposure assessments of SOx, NOx PM10/2.5 and trace metals from oil industries: a review study (2000–2018), Process Saf. Environ. Protect. 123 (2019) 215–228.
[3] R. Grazuleviciene, L. Maroziene, V. Dulskiene, V. Malinauskiene, A. Azaraviciene, D. Laurinaviciene, et al., Exposure to urban nitrogen dioxide pollution and the risk of myocardial infarction, Scand. J. Work. Environ. Health 30 (4) (2004) 293–298.
[4] M. Cano, F. Guarín, B. Aristizábal, A.-L. Villa, L.-M. González, Catalytic activity and stability of Pd/Co catalysts in simultaneous selective catalytic reduction of NOx with methane and oxidation of o-dichlorobenzene, Catal. Today 296 (2017) 105–117.
[5] H. Zhao, P. Meng, S. Gao, Y. Wang, P. Sun, Z. Wu, Recent advances in simultaneous removal of NOx and VOCs over bifunctional catalysts via SCR and oxidation reaction, Sci. Total Environ. 906 (2024) 167553.
[6] J.-F. Gelves, L. Dorkis, M.-A. Márquez, A.-C. Álvarez, L.-M. González, A.-L. Villa, Activity of an iron Colombian natural zeolite as potential geo-catalyst for NH_3-SCR of NOx, Catal. Today 320 (2019) 112–122.
[7] K. Elghniji, J. Soro, S. Rossignol, M. Ksibi, A simple route for the preparation of P-modified TiO2: effect of phosphorus on thermal stability and photocatalytic activity, J. Taiwan Inst. Chem. Eng. 43 (1) (2012) 132–139.
[8] G. Lofrano, G. Libralato, A. Casaburi, A. Siciliano, P. Iannece, M. Guida, et al., Municipal wastewater spiramycin removal by conventional treatments and heterogeneous photocatalysis, Sci. Total Environ. 624 (2018) 461–469.
[9] P. Pichat, A brief survey of the practicality of using photocatalysis to purify the ambient air (indoors or outdoors) or air effluents, Appl. Catal., B 245 (2019) 770–776.
[10] Z. Shayegan, C.-S. Lee, F. Haghighat, TiO_2 photocatalyst for removal of volatile organic compounds in gas phase – a review, Chem. Eng. J. 334 (2018) 2408–2439.
[11] J. Ángelo, L. Andrade, L.M. Madeira, A. Mendes, An overview of photocatalysis phenomena applied to NOx abatement, J. Environ. Manag. 129 (2013) 522–539.
[12] Y. Boyjoo, H. Sun, J. Liu, V.K. Pareek, S. Wang, A review on photocatalysis for air treatment: from catalyst development to reactor design, Chem. Eng. J. 310 (2017) 537–559.
[13] R. Zouzelka, J. Rathousky, Photocatalytic abatement of NOx pollutants in the air using commercial functional coating with porous morphology, Appl. Catal., B 217 (2017) 466–476.
[14] N. Todorova, T. Giannakopoulou, K. Pomoni, J. Yu, T. Vaimakis, C. Trapalis, Photocatalytic NOx oxidation over modified ZnO/TiO_2 thin films, Catal. Today 252 (2015) 41–46.
[15] N. Todorova, T. Giannakopoulou, S. Karapati, D. Petridis, T. Vaimakis, C. Trapalis, Composite TiO_2/clays materials for photocatalytic NOx oxidation, Appl. Surf. Sci. 319 (2014) 113–120.
[16] A. Martinez-Oviedo, S.K. Ray, H.P. Nguyen, S.W. Lee, Efficient photo-oxidation of NOx by Sn doped blue TiO_2 nanoparticles, J. Photochem. Photobiol. Chem. 370 (2019) 18–25.
[17] M. Bellardita, A. Di Paola, L. Palmisano, F. Parrino, G. Buscarino, R. Amadelli, Preparation and photoactivity of samarium loaded anatase, brookite and rutile catalysts, Appl. Catal., B 104 (3) (2011) 291–299.
[18] Q.-Y. Luo, H. Luo, H.-M. Kuang, W.-T. Chen, Y.-X. Wen, A novel samarium material: synthesis, structure, photophysical properties and photoluminescence energy transfer mechanism, J. Solid State Chem. 270 (2019) 200–204.
[19] A.J. Moreira, D. Coelho, J.A. Dias, L.H. Mascaro, G.P.G. Freschi, V.R. Mastelaro, et al., Phase control and optimization of photocatalytical properties of samarium doped TiO_2 synthesized by coupled ultraviolet and microwave radiations, J. Alloys Compd. 905 (2022) 164217.
[20] D.J. Park, T. Sekino, S. Tsukuda, A. Hayashi, T. Kusunose, S.-I. Tanaka, Photoluminescence of samarium-doped TiO_2 nanotubes, J. Solid State Chem. 184 (10) (2011) 2695–2700.

[21] Y. Qin, Z. Hu, B.H. Lim, W.S. Chang, K.K. Chong, P. Zhang, et al., Sol-hydrothermal synthesis of TiO_2:Sm^{3+} nanoparticles and their enhanced photovoltaic properties, J. Alloys Compd. 686 (2016) 803–809.
[22] S. Rajoriya, S. Bargole, S. George, V.K. Saharan, P.R. Gogate, A.B. Pandit, Synthesis and characterization of samarium and nitrogen doped TiO_2 photocatalysts for photo-degradation of 4-acetamidophenol in combination with hydrodynamic and acoustic cavitation, Sep. Purif. Technol. 209 (2019) 254–269.
[23] J.C. Arévalo-Pérez, D. De la Cruz-Romero, A. Cordero-García, C.E. Lobato-García, A. Aguilar-Elguezabal, J.G. Torres-Torres, Photodegradation of 17 α-methyltestosterone using TiO_2-Gd^{3+} and TiO_2-Sm^{3+} photocatalysts and simulated solar radiation as an activation source, Chemosphere 249 (2020) 126497.
[24] D. De la Cruz, J. Arevalo-Pérez, J. Torres Torres, R. Bautista Margulis, C. Ornelas, A. Aguilar-Elguezabal, TiO_2 doped with Sm^{3+} by sol–gel: synthesis, characterization and photocatalytic activity of diuron under solar light Catal Today 166 (1) (2011) 152–158.
[25] S. Asal, M. Saif, H. Hafez, S. Mozia, A. Heciak, D. Moszyński, et al., Photocatalytic generation of useful hydrocarbons and hydrogen from acetic acid in the presence of lanthanide modified TiO_2, Int. J. Hydrogen Energy 36 (11) (2011) 6529–6537.
[26] H. Peng, R. Guo, H. Lin, Photocatalytic reduction of CO_2 over Sm-doped TiO_2 nanoparticles, J. Rare Earths 38 (12) (2020) 1297–1304.
[27] J. Tang, X. Chen, Y. Liu, W. Gong, Z. Peng, T. Cai, et al., Samarium-doped mesoporous TiO_2 nanoparticles with improved photocatalytic performance for elimination of gaseous organic pollutants, Solid State Sci. 15 (2013) 129–136.
[28] Paola A. Di, M. Bellardita, G. Marcì, L. Palmisano, F. Parrino, R. Amadelli, Preparation of Sm-loaded brookite TiO2 photocatalysts, Catal. Today 161 (1) (2011) 35–40.
[29] M. Chang, Y. Song, J. Chen, X. Zhang, D. Meng, H. Zhu, et al., Multisite luminescence and photocatalytic properties of TiO_2:Sm^{3+} and TiO^2:Sm^{3+}@TiO_2/TiO_2:Sm^{3+}@SiO_2 luminescent enhancement materials, J. Alloys Compd. 725 (2017) 724–738.
[30] A. Kutuzova, J.-O. Moritz, N.G. Moustakas, T. Dontsova, T. Peppel, J. Strunk, Performance of Sm-doped TiO_2 in photocatalytic antibiotic degradation and photocatalytic CO_2 reduction, Appl. Nanosci. 13 (10) (2023) 6951–6966.
[31] J.C. Arévalo-Pérez, G. Torres-Torres, D. De la Cruz-Romero, H. Perez-Vidal, M. A. Lunagomez-Rocha, I. Cuauhtémoc-Lóipez, et al., Photocatalytic treatment of pesticides using TiO_2 doped with rare earth, in: E. Murat (Ed.), Water and Wastewater Treatment, IntechOpen, Rijeka, 2019. Ch. 7.
[32] E. Luévano-Hipólito, A. Martínez de la Cruz, Enhancement of photocatalytic properties of TiO_2 for NO photo-oxidation by optimized sol–gel synthesis, Res. Chem. Intermed. 42 (9) (2016) 7065–7084.
[33] ISO I.S.O. ISO 22197-2016 Fine Ceramics (Advanced Ceramics, Advanced Technical Ceramics) — Test Method for Air-Purification Performance of Semiconducting Photocatalytic Materials — Part 1: Removal of Nitric Oxide, ISO, Zurich, Switzerland, 2016, p. 13.
[34] S.L. Isley, R.L. Penn, Relative brookite and anatase content in Sol−Gel-synthesized titanium dioxide nanoparticles, J. Phys. Chem. B 110 (31) (2006) 15134–15139.
[35] Y. Li, T.J. White, S.H. Lim, Low-temperature synthesis and microstructural control of titania nano-particles, J. Solid State Chem. 177 (4) (2004) 1372–1381.
[36] F. Méndez-Arriaga, M. Maldonado, J. Giménez, S. Esplugas, S. Malato, Abatement of ibuprofen by solar photocatalysis process: enhancement and scale up, Catal. Today 144 (2009) 112–116.
[37] K.M. Parida, N. Sahu, Visible light induced photocatalytic activity of rare earth titania nanocomposites, J. Mol. Catal. Chem. 287 (1) (2008) 151–158.
[38] A. Arce-Sarria, F. Machuca-Martínez, C. Bustillo-Lecompte, A. Hernández-Ramírez, J. Colina-Márquez, Degradation and loss of antibacterial activity of commercial amoxicillin with TiO_2/WO_3-assisted solar photocatalysis, Catalysts 8 (6) (2018).
[39] H. Eskandarloo, A. Badiei, M.A. Behnajady, G.M. Ziarani, Ultrasonic-assisted sol–gel synthesis of samarium, cerium co-doped TiO_2 nanoparticles with enhanced sonocatalytic efficiency, Ultrason. Sonochem. 26 (2015) 281–292.
[40] H.T. Gao, W.C. Liu, G.J. Liu, Facile synthesis and enhanced photocatalysis of Sm doped TiO_2, Adv. Mater. Res. 490–495 (2012) 3272–3276.
[41] V. Štengl, S. Bakardjieva, N. Murafa, Preparation and photocatalytic activity of rare earth doped TiO_2 nanoparticles, Mater. Chem. Phys. 114 (1) (2009) 217–226.
[42] D. Sun, K. Wang, Z. Xu, R. Li, Synthesis and photocatalytic activity of sulfate modified Nd-doped TiO_2 under visible light irradiation, J. Rare Earths 33 (5) (2015) 491–497.
[43] C. Fan, P. Xue, Y. Sun, Preparation of nano-TiO_2 doped with cerium and its photocatalytic activity, J. Rare Earths 24 (3) (2006) 309–313.
[44] A.-W. Xu, Y. Gao, H.-Q. Liu, The preparation, characterization, and their photocatalytic activities of rare-earth-doped TiO_2 nanoparticles, J. Catal. 207 (2) (2002) 151–157.
[45] S. Li, Y. Yang, Q. Su, X. Liu, H. Zhao, Z. Zhao, et al., Synthesis and photocatalytic activity of transition metal and rare earth element co-doped TiO_2 nano particles, Mater. Lett. 252 (2019) 123–125.
[46] S. Wang, Z. Wang, Y. Wang, C. Xia, E. Hong, L. Bai, et al., Study on the controlled synthesis and photocatalytic performance of rare earth Nd deposited on mesoporous TiO_2 photocatalysts, Sci. Total Environ. 652 (2019) 85–92.
[47] H. Shi, T. Zhang, H. Wang, Preparation and photocatalytic activity of La^{3+} and Eu^{3+} co-doped TiO_2 nanoparticles: photo-assisted degradation of methylene blue, J. Rare Earths 29 (8) (2011) 746–752.
[48] Q. Xiao, Z. Si, Z. Yu, G. Qiu, Sol–gel auto-combustion synthesis of samarium-doped TiO_2 nanoparticles and their photocatalytic activity under visible light irradiation, Materials Science and Engineering: B. 137 (1) (2007) 189–194.
[49] A. Wang, Q. Wu, C. Han, H. Yang, X. Xue, Significant influences of crystal structures on photocatalytic removal of NOx by TiO_2, J. Photochem. Photobiol. Chem. 407 (2021) 113020.
[50] E. Luévano-Hipólito, Martínez-de la Cruz A. Photocatalytic stucco for NOx removal under artificial and by real weatherism, Construct. Build. Mater. 174 (2018) 302–309.